Crossing the elliptic region in a hyperbolic system with change-of-type behavior arising in flow between two parallel plates

L. Talon, J. Martin, N. Rakotomalala, and D. Salin
FAST, Universités Paris VI et Paris XI, CNRS (UMR 7608), Bâtiment 502, Campus Universitaire, 91405 Orsay Cedex, France

Y. C. Yortsos
Department of Chemical Engineering, University of Southern California, Los Angeles, California 90089-1211, USA
(Received 16 December 2003; revised manuscript received 23 March 2004; published 24 June 2004)

Change-of-type behavior from hyperbolic to elliptic is common to quasilinear hyperbolic systems. This issue is addressed here for the particular case of miscible flow of three fluids between two parallel plates. Change of type occurs at the leading edge of the displacement front and reflects the failing of the equilibrium assumption, necessary for the quasilinear hyperbolic formalism, at the front. To cross the elliptic region requires the solution of the full, higher-dimensionality problem, obtained here using lattice gas simulations. For the specific example, it is found that the system self-selects a front structure independent of injection conditions.

DOI: 10.1103/PhysRevE.69.066318 PACS number(s): 47.55.Mh, 47.15.Gf, 02.30.Jr, 47.54.+r

Moving fronts are encountered in many processes in science and engineering. Often, the geometries involve a large aspect ratio and it is common to seek a scaled-up formulation, using quantities averaged across the directions y,z transverse to the main flow direction x. For example, this is the case with fluid displacements in constricted geometries, or porous media, in the flow of suspensions, in combustion, and in a number of applications where kinematics are dominant [1–5].

Under these conditions, the modeling of the problem is based on conservation equations in terms of volume or transverse averages, typically reducing to quasilinear hyperbolic systems of the form

$$\frac{\partial \mathbf{S}}{\partial t} + \frac{\partial \mathbf{F}(\mathbf{S})}{\partial x} = \mathbf{0}. \tag{1}$$

In Eq. (1), $\mathbf{S}$ denotes an averaged "concentration" or "saturation" (volume fraction), in general a vector of size N, and $\mathbf{F}$ is an averaged flux, also a vector of the same size. For example, in three-phase flows in a porous medium, $\mathbf{S}=\{S_1,S_2\}$, where S_i is the saturation of phase i (the third saturation being $1-S_1-S_2$). In the sedimentation of bidisperse suspensions, $\mathbf{S}$ is the concentration vector of the two species. Corresponding expressions apply for the more commonly known problems in gas dynamics and the flow of real materials (e.g., see [6]).

The space and time evolution of $\mathbf{S}$ is given by

$$\frac{\partial \mathbf{S}}{\partial t} + \mathbf{A}(\mathbf{S})\frac{\partial \mathbf{S}}{\partial x} = \mathbf{0}, \tag{2}$$

where the matrix $\mathbf{A}$ is equal to $\mathbf{A}=d\mathbf{F}/d\mathbf{S}$. For $N=2$, matrix $\mathbf{A}$ has two eigenvalues λ_- and λ_+. The classical construction of the solution of a Riemann problem is well understood [7]. When both eigenvalues are real, the system is hyperbolic. The solution of a Riemann problem, in this case, is a combination of rarefaction waves and shocks: In the composition diagram ($\{S_1,S_2\}$ space), rarefaction waves follow continuous paths obtained from the integral solutions of the right eigenvectors corresponding to λ_- or λ_+. Shocks represent discontinuous jumps between two compositions and satisfy the Rankine-Hugoniot conditions. If in a region of composition space the eigenvalues are complex, the system is elliptic. Batchelor and Van Rensburg [2] showed that any uniform state $\mathbf{S}$ in the elliptic domain is unstable and used this fact to classify stable and unstable bidisperse suspensions. Analogous results were found by Bell *et al.* [8] in the context of three-phase flow in porous media. Key issues, studied at length in the past [8–11], but not yet fully resolved, include the solution of Riemann problems involving both hyperbolic and elliptic domains in the $\{S_1,S_2\}$ space. Methods have been proposed to cross the elliptic domain involving a shock between two compositions in the hyperbolic domain or the addition of diffusion [12]. The latter requires large enough diffusion to either stabilize the pattern or bypass the elliptic region, thus changing the nature of the problem.

There has been a debate as to whether or not the change of type (from hyperbolic to elliptic) and the associated Riemann problems that cross the elliptic region are physically relevant. Part of the difficulty lies in the fact that, so far, models exhibiting such a change of type have been based on empirical functions $\mathbf{F}(\mathbf{S})$. In fact, some authors have argued that the appearance of an elliptic region should be sufficient grounds to reject the particular empiricism used to construct the function $\mathbf{F}(\mathbf{S})$ and to provide alternate (albeit still empirical) expressions, for which an elliptic region does not develop [13,14]. A different viewpoint is that shocks across elliptic regions are not classical, but rather result from the solution of eigenvalue problems in the shock region, where additional terms of higher-order than diffusion (e.g., capillarity) must be taken into account [7,15,16].

In this article we show that a physical model, without any empirical functions whatsoever, can give rise to a hyperbolic formalism displaying change of type. The model corresponds to laminar miscible fluid flow in the gap of a Hele-Shaw cell at high rates [17–20]. A fluid of normalized viscosity 1 is displaced by a fluid of normalized viscosity Λ^{-1} (mobility

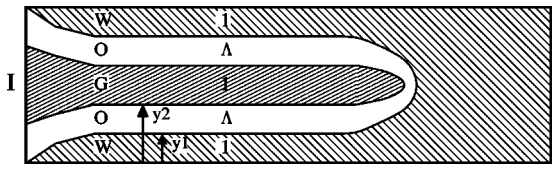

FIG. 1. Schematics of the boundaries between the three fluids (W,O,G) and their corresponding mobilities (1, Λ, 1) for a specific Riemann problem (denoted by state *I* in Fig. 2). Injection state at left, initial state at right. Flow and displacement are from left to right.

Λ), which is itself displaced by a fluid of viscosity 1 (Fig. 1). Under parallel-flow conditions (namely, using the lubrication approximation), a hyperbolic formalism describes the problem, as shown below. We show that when $\Lambda>1$, an elliptic region develops at the front of the displacement, resulting in a mixed-type problem. To solve the problem in the latter case near the front, we use lattice Bhatnagar-Gross-Krook (BGK) simulations [21] of the full two-dimensional flow. The results obtained are discussed in the frame of the quasilinear formalism and nonclassical shocks [7].

Consider a miscible displacement in the gap of a Hele-Shaw cell (*x*-*y* plane) and in the absence of gravity, as shown in Fig. 1. A symmetric displacement across the gap is considered. Three different miscible fluids, denoted *W*, *O*, and *G*, are involved. The cell, of normalized thickness 1, is initially saturated with fluid *W* (downstream in Fig. 1). Two other fluids (*O*, denoting an intermediate fluid, and *G*) are injected at constant rate and specified saturations (upstream in Fig. 1) to displace fluid *W*. In the absence of diffusion, the problem is strictly kinematic and can be equivalently formulated as miscible displacement involving one variable, the local concentration *C*, with the three different fluids identified by their mobility. For the latter, we take a piecewise mobility-concentration function involving three plateaus, with the corresponding concentration regions defining the three fluids—i.e., region $0<C<0.25$ $(0<y<y_1$, Fig. 1) is the *W* fluid with mobility 1, region $0.25<C<0.75$ $(y_1<y<y_2)$ is the *O* fluid with mobility Λ, and region $0.75<C<1$ $(y_2<y<1/2)$ is the *G* fluid with mobility *M*. In this paper we will only consider the case $M=1$.

We study the evolution of the boundaries y_1 and y_2 that separate the three fluids (Fig. 1). Equivalently, we can use the saturation notation $S_w=2y_1$, $S_g=1-2y_2$, and $S_o=1-S_w-S_g$. It is not difficult to write conservation equations

$$\frac{\partial S_w}{\partial t}+\frac{\partial f_w}{\partial x}=0,$$

$$\frac{\partial S_g}{\partial t}+\frac{\partial f_g}{\partial x}=0, \tag{3}$$

where we defined the associated normalized flux functions $f_w=2\int_0^{y_1} u dy$ and $f_g=1-2\int_0^{y_2} u dy$ (and in this notation, $f_o=1-f_w-f_g$). In general, the flux functions are nonlocal and depend on both saturations and possibly their derivatives or other functionals. When the flow is parallel or nearly parallel (lubrication approximation), however, the fluxes become

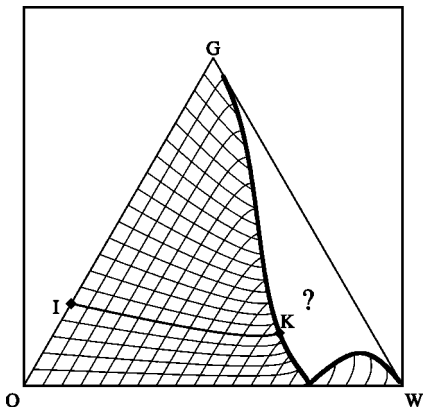

FIG. 2. Composition paths in the triangular composition diagram for $\Lambda=10$. Apexes G,O, and W correspond to $S_g=1$, $S_o=1$, and $S_w=1$, respectively. A region of ellipticity, denoted by "?," develops near the *GW* axis. The curves in the hyperbolic part are solution paths corresponding, respectively, to the eigenvalues λ_- and λ_+. Point *I* denotes the injection state and point *W* the initial state for the Riemann problem considered. Path *IK* is the rarefaction wave corresponding to eigenvalue λ_-.

only functions of the two saturations, and the formalism (3) reduces to the quasilinear expression (1). Specifically, we find

$$f_w=\frac{S_w^2(3-S_w)}{2[1+(\Lambda-1)(1-S_w)^3-(\Lambda-1)S_g^3]},$$

$$f_g=\frac{S_g[3+3(\Lambda-1)(1-S_w)^2+S_g^2(2-3\Lambda]}{2[1+(\Lambda-1)(1-S_w)^3-(\Lambda-1)S_g^3]}. \tag{4}$$

These expressions are obtained by transversely averaging the Stokes equations across the gap under the assumption of parallel flow. The procedure was illustrated for the two-fluid problem in [20,22], and although a bit tedious, it is straightforward. We emphasize that the parallel-flow approximation is necessary for consistency of the quasilinear formalism (1) at steady state, where indeed the flow is parallel. This assumption can also be viewed as the equivalent of the equilibrium or quasistatic assumption made in thermodynamics in other contexts—for example, in the equation of state in the flow of a van der Waals fluid [15].

From the exact expressions for the flux (4) we can readily calculate the two eigenvalues λ_- (slow) and λ_+ (fast). It is found that when the mobility of the intermediate fluid, Λ, is smaller than 1, the system is hyperbolic (two real eigenvalues). In the opposite case $(\Lambda>1)$, the eigenvalues become complex in a region adjacent to the *WG* axis (Fig. 2), and the system displays a change of type from hyperbolic to elliptic in the composition space. The considerable details of this calculation can be found in [23]. Condition $\Lambda>1$ physically corresponds to the case of a concave mobility profile, where a more viscous initial fluid is being displaced by an intermediate, less viscous fluid, which is itself being displaced by a more viscous fluid. Nonmonotonic viscosity profiles have led

to interesting behaviors in porous media flows (e.g., see [24–26]). However, the latter were based on Darcy rather than Stokes flows.

We will consider the solution of various Riemann problems using injection states along the axis *OG* and an initial state at point *W* and discuss the results in a triangular composition space (Fig. 2). As noted, in our example we have either a hyperbolic system ($\Lambda<1$) or a mixed-type case ($\Lambda>1$). In the latter case, both elliptic and hyperbolic regions are encountered. For the specific Riemann problem, in the hyperbolic case, or within the hyperbolic regions, the solution involves rarefaction waves, which follow the paths depicted in Fig. 2 (two sets corresponding to the two eigenvalues). The classical analytical theory fails to give an answer about the behavior of the system in the elliptic zone (denoted by "?" in Fig. 2). The solution to this issue will be addressed in this paper. We stress again that the development of an elliptic region arises here in the absence of *any* empirical assumptions. It is based on the parallel-flow (lubrication) approximation, which is required for self-consistency of the quasilinear formalism, and on the nonmonotonicity in the mobility profile.

Consider, first, the solution of a Riemann problem, with injection at point *I* and initial condition at *W* (Fig. 2 with $\Lambda=10$). Because of the mixed-type behavior, analytical results are possible in the hyperbolic part of the composition diagram (Fig. 2). In that region, the two sets of composition paths (solutions of Riemann problem) terminate at the boundary of the elliptic region, where their slopes become equal. Noteworthy is the development of a lobe of genuine hyperbolicity near the apex *W*. The analytical construction follows the slow λ_- path *IK*, and it is a rarefaction wave, terminating when the path meets the elliptic region boundary, at point *K*. Connection to the initial state *W* requires crossing of the elliptic region. This coincides with the leading part of the displacement front and cannot be handled by classical analytical methods. To proceed, we simulated the *full*, higher-dimensional problem using a lattice BGK method.

Lattice BGK methods effectively model, over the full domain, the Navier-Stokes equations for momentum balance, the overall mass balance, and the convection-diffusion equation for the transport of concentration, as the three fluids are miscible. We note that in dimensionless notation, the mass transport equation reads

$$\frac{\partial C}{\partial t}+\frac{\partial (uC)}{\partial x}+\frac{\partial (vC)}{\partial y}=D\left[\epsilon^2\frac{\partial^2 C}{\partial x^2}+\frac{\partial^2 C}{\partial y^2}\right], \qquad (5)$$

where $\epsilon=H/L$ is the aspect ratio, u and v are the two velocity components, and D is a dimensionless molecular diffusion coefficient (an inverse Peclet number), which was chosen very small to minimize diffusion effects in accordance with the kinematic description. Lattice BGK methods have been successfully used in the past in simulating the corresponding two-fluid displacement problem. Indeed, a good agreement was found between experiments [17–20] and simulations [21]. The same approach was applied here, except that we used the piecewise mobility concentration function discussed above to define the three fluids.

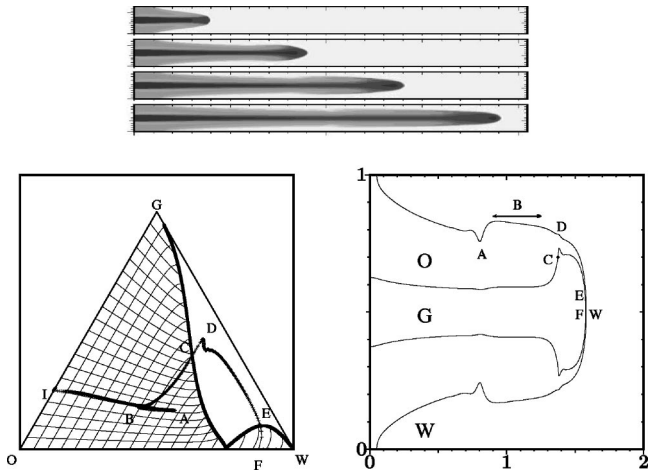

FIG. 3. Lattice BGK simulation results for the Riemann problem of Fig. 2. Top: snapshots of the three-fluid displacement at different times. Bottom left: the solution path on the composition diagram. Bottom right: fluid boundaries as a function of the convective variable x/t (effectively collapsing the latter stages of the top panel). The detail at point *A* is probably the result of weak inertia, which is present in the simulations, but absent in the analytical description.

Results from the simulations are shown in Fig. 3. The top panel shows successive snapshots of the displacement pattern, the bottom left panel displays the solution path in the composition diagram, and the bottom right panel displays the fluid boundaries as a function of the convective variable x/t. The following features are noted.

(i) Due to diffusion, no matter how small, the most downstream part of the profile consists of a two-fluid path *FW*, connecting points *W* and *F*. The latter point has a value $S_o \approx 0.1$, which varies with the diffusion coefficient. *FW* corresponds to the leading edge of the front, moving in real space (Fig. 3, top) with a velocity slightly larger than $3/2$ (which is the maximum normalized velocity in a Poiseuille flow). We note that this velocity is consistent with the shock velocity of the two-fluid problem with $M=10$ and states *F* and *W*, respectively [21,22].

(ii) Slightly further upstream, the trajectory follows the path *EF* with an almost constant velocity. It appears as if the composition *E* is selected such that the velocity on *EF* matches the shock velocity *FW*, while satisfying the Rankine-Hugoniot condition for a shock in the hyperbolic lobe. If so, that would be consistent with a quasilinear formalism in that region.

(iii) The system then locks into a path *ED*, which is inside the elliptic region. Of course, it must be kept in mind that these results are obtained from the solution of the full, higher-dimensional problem. The saturation of fluid *O* remains approximately constant, at a value that depends on the diffusion coefficient (and which in theory should vanish), but that of fluid *G* increases in the upstream direction until a maximum value is reached. Along *ED*, the finger of phase *G* swells up to an almost uniform thickness (see bottom right panel in Fig. 3).

(iv) State *D* is then connected upstream with the hyper-

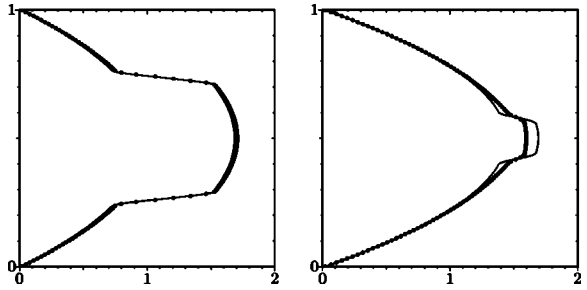

FIG. 4. Profiles of the x component of the velocity, corresponding to points D and E in the diagram of Fig. 3. Left: profile at a position close to point D. Right: profile at point E. Dots denote simulation results using the full problem; lines correspond to the parallel-flow (equilibrium) assumption.

bolic solution at point B, through a shock, corresponding to the fast eigenvalue. The shock velocity is consistent with the quasilinear hyperbolic formulation. Across this shock, the saturation of fluid G decreases upstream, while that of fluid O increases.

(v) Finally, state B is connected further upstream to the injection state I, following the hyperbolic formalism. In the simulations, we noted that after some transient time there appears to be a reversal along path AB (as shown in Fig. 3). Namely, although the saturation of fluid O first decreases monotonically, after some time, a nonmonotonic segment AB develops, along which the saturation increases instead. During this process, the saturation of fluid G is practically constant. It is not clear that this is a real feature of the viscous problem, however. It is possible, instead, that it is an artifact of the weak inertia, which is present in the lattice BGK model and which may result into an instability.

The states along the paths BF are all located at the leading edge of the displacement front, near, or inside the elliptic region, where saturation gradients are non-negligible. In that region the equilibrium (parallel-flow) approximation may be questionable. To probe the validity of the latter we plot in Fig. 4 the profile of the x component of the velocity at points D and E, and compare it to that based on the parallel-flow assumption. In the vicinity of point D, where the saturation gradient is relatively small, the two profiles are in good agreement (Fig. 4, left). However, at point E at the leading edge of the front, there is a clear deviation (Fig. 4, right), indicating considerable cross flow, associated with the non-negligible front curvature at that point. In the transition from points D to E, the deviation progressively increases.

Figure 5 shows lattice BGK simulations for the same mixed-type case ($\Lambda = 10$) but for three different Riemann problems, corresponding to different injection conditions. As expected, in all cases, the solution path in the hyperbolic region follows the hyperbolic theory (although augmented with some amount of diffusion, particularly for the case in which injection occurs at point G), and it is different for the three different problems. Yet the path through the elliptic

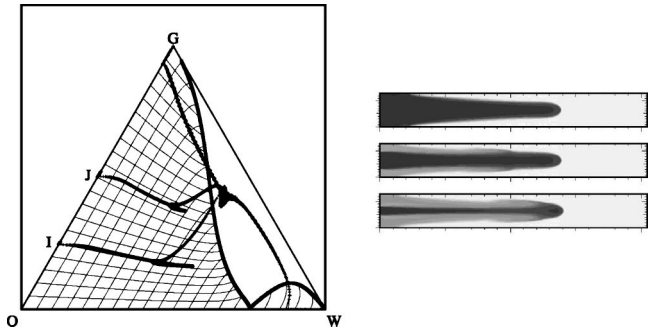

FIG. 5. Lattice BGK simulation results for three different Riemann problems, corresponding to three injection conditions at I, J, and G, respectively. Left: solution paths in the composition space. Right: snapshots of the three-fluid patterns, at the same time, for the three different injection points I, J, and G. As before, the tip resides inside the elliptic region in all cases. The selection of the tip structure is independent of the injection state.

zone is the same for all three problems and practically *independent* of the injection state. The front structure is set by the detailed two-dimensional flow at the front (right panel Fig. 5). Hyperbolic and elliptic paths are connected through intermediate connecting branches (e.g., of the type DB of Fig. 3). We infer that the behavior of the front is selected from the full, higher-dimensional local problem, independent of the injection conditions. This feature is not predictable from classical shock analysis, in which the front structure is simply endowed with a so-called "viscosity" correction, adding a diffusive component (e.g., as in the classical Burgers shock [7]). Instead, it is consistent with nonclassical shock theories [7,16], in which the shock-end points, the shock structure, and its velocity are obtained from the solution of an eigenvalue problem, developed from the addition of higher-order dispersive terms—e.g., due to some effective capillarity. The possible connection with such an approach is the subject of ongoing research.

We conclude that in the present example of change of type behavior, the elliptic region develops precisely at the tip of the displacement, where the variables undergo sharp changes (effectively a "phase change") and where the parallel-flow (equilibrium) assumption breaks down. The emergence of a mixed-type region is a manifestation of the local failure of the parallel-flow approximation, which is necessary for the development of the quasilinear hyperbolic formalism. Crossing the elliptic region cannot be given by the classical quasilinear hyperbolic formalism, which is questionable in that region, however. Rather, obtaining the structure, including the velocity and end points, of the solution necessitates solving the full, higher-dimensional problem in that region.

This may signal a nonclassical shock construction [7]. Whether or not a simpler alternative to the solution of the full problem is possible is the subject of ongoing work.

[1] L. Lake, *Enhanced Oil Recovery* (Prentice Hall, Englewood Cliffs, NJ, 1989).
[2] G. Batchelor and R. Janse Van Rensburg, J. Fluid Mech. **166**, 379 (1985).
[3] A. Aldushin and B. Matkowsky, Combust. Sci. Technol. **133**, 293 (1998).
[4] P. Pelcé, *Dynamics of Curved Fronts* (Academic Press, Boston, 1988).
[5] J. Martin, N. Rakotomalala, and D. Salin, Phys. Fluids **7**, 2510 (1995).
[6] R. Menikoff and B. Plohr, Rev. Mod. Phys. **61**, 75 (1989).
[7] P. LeFloch, *Hyperbolic Systems of Conservation Laws* (Birkhauser Verlag, Basel, 2002).
[8] J. Bell, J. Trangenstein, and G. Shubin, SIAM (Soc. Ind. Appl. Math.) J. Appl. Math. **46**, 1000 (1986).
[9] E. Isaacson, D. Marchesin, and B. Plhor, SIAM J. Math. Anal. **21**, 837 (1990).
[10] B. Keyfitz, J. Diff. Eqns. **80**, 280 (1989).
[11] M. Shearer and J. Trangenstein, Transp. Porous Media **4**, 499 (1989).
[12] D. Jackson and M. Blunt, Transp. Porous Media **48**, 249 (2002).
[13] R. Juanes and T. Patzek, Transp. Porous Media (to be published).
[14] F. Fayers and J. Matthews, SPEJ **24**, 225 (1984).
[15] L. Truskinovskii, J. Appl. Math. Mech. **51**, 777 (1987).
[16] M. Shearer and Y. Yang, Proc. - R. Soc. Edinburgh, Sect. A: Math. **125**, 675 (1995).
[17] P. Petitjeans and T. Maxworthy, J. Fluid Mech. **326**, 37 (1996).
[18] C.-Y. Chen and E. Meiburg, J. Fluid Mech. **326**, 57 (1996).
[19] E. Lajeunesse, J. Martin, N. Rakotomalala, and D. Salin, Phys. Rev. Lett. **79**, 5254 (1997).
[20] E. Lajeunesse, J. Martin, N. Rakotomalala, D. Salin, and Y. C. Yortsos, J. Fluid Mech. **398**, 299 (1999).
[21] N. Rakotomalala, D. Salin, and P. Watzky, J. Fluid Mech. **338**, 277 (1997).
[22] Z. Yang and Y. C. Yortsos, Phys. Fluids **9**, 286 (1997).
[23] M. Shariati, L. Talon, J. Martin, N. Rakotomalala, D. Salin, and Y. C. Yortsos (unpublished).
[24] F. Manickam and G. Homsy, Phys. Fluids A **5**, 1356 (1993).
[25] D. Loggia, N. Rakotomalala, and D. Salin, Phys. Fluids **11**, 740 (1999).
[26] M. Shariati and Y. C. Yortsos, Phys. Fluids **13**, 2245 (2001).